Bol. Soc. Paran. Mat.
©SPM – E-ISSN-2175-1188
SPM: www.spm.uem.br/bspm

(3s.) **v. 2025 (43) 2** : 1–12.
ISSN-0037-8712
doi:10.5269/bspm.78988

Boundary layer flow of a Walter's B fluid driven by a stretching cylinder with viscosity influenced by temperature and concentration variations

Annwesha Borthakur* and Debasish Dey

ABSTRACT: The present work investigates the heat and mass transfer in a steady boundary layer flow of a Walter's B fluid driven by a stretching cylinder, taking into account the effects of temperature-and concentration-dependent variable viscosity. The primary goal is to analyze the flow under free convection, incorporating the Rosseland approximation to model thermal radiation, which constitutes a novelty of the work. By employing similarity transformations, the governing equations are reduced to a system of nonlinear ordinary differential equations. A comprehensive analysis of the variations in velocity, temperature, and concentration is conducted through numerical simulations for different flow-related parameters. In addition, the skin friction coefficient (C_f), Nusselt number (N_u), and Sherwood number (S_h) are evaluated. It is observed that an increase in the Stefan–Boltzmann constant (σ) and the mean absorption coefficient (k) reduces the fluid temperature.

Key Words: Stretching cylinder, variable viscosity, Walter's B fluid, thermal radiation.

Contents

1. Introduction

In many studies of fluid dynamics, viscosity is often treated as a constant. However, this assumption is not valid in all scenarios, as viscosity can depend on variables such as temperature, pressure, or spatial location. For instance, in the case of coal slurries, viscosity is known to change with temperature. Crude oil becomes less viscous at higher temperatures, which is why heating is often used during transportation to improve flow [1]. Likewise, in various thermal transport processes, non-uniform temperature distribution across the flow field can cause notable variations in viscosity, particularly under conditions involving large temperature gradients. Unlike Newtonian fluids such as water and air, where viscosity remains constant regardless of the applied shear rate, non-Newtonian fluids exhibit viscosity changes in response to varying shear rates. While their viscosity also decreases with rising temperature, similar to Newtonian fluids, this decline can have a notable impact on manufacturing processes [2]. Considering the flow of an incompressible, thermodynamically compatible grade three fluid through a uniform pipe Massoudi and Christie [3] explored the effects of variable viscosity and viscous dissipation of the flow. They assumed that the pipe's temperature exceeded that of the fluid and that the fluid's shear viscosity depended on temperature variations. Using the homotopy analysis method (HAM), Hayat et al. [4] presented an analytical solution for the flow of a grade three fluid in a pipe. Variable space dependence viscosity is considered in that context and the temperature of the pipe is taken to be higher than the temperature of the fluid. Subsequently, Yursoy and Pakdemirili [5], as well as Pakdemirili and Yilbas [6], investigated the approximate and analytical solutions for non-Newtonian fluids with variable viscosity. Under no-slip scenarios, Nadeem and Ali [7] analysed the stable, incompressible flow of a fourth-grade fluid up a vertical cylinder while considering heat transfer and varying viscosity into account. Later, employing two viscosity models—the Reynold's and Vogel's models—Nadeem et al. [8] explored the flow and heat transfer

* Corresponding author.
2010 *Mathematics Subject Classification:* 76A10, 76A05, 76D10.
Submitted September 15, 2025. Published November 01, 2025

Typeset by $\mathcal{B}^{S}\mathcal{P}_{\mathcal{M}}$ style.
© Soc. Paran. de Mat.

aspects of a fourth-grade fluid with varying viscosity under partial slip settings. The flow, driven by a constant pressure gradient, accounted for partial slip effects at the cylinder wall. Later, Nadeem and Akbar [9] investigated how temperature-dependent viscosity influenced a Jeffrey-six steady fluid's peristaltic flow in a uniform vertical tube. They utilized the homotopy analysis approach and the regular perturbation method to solve the governing equations for axial pressure gradient, temperature, and velocity profile. Non-Newtonian viscosity often depends simultaneously on both temperature and concentration across various systems. For instance, lung surfactant dispersions, such as lavaged calf lung surfactant (LS) and its chloroform-methanol extract (CLSE), show increased viscosity with higher phospholipid concentrations and exhibit non-Newtonian behavior, with viscosity varying significantly between 23°C, 37°C, and 10°C [10]. Similarly, aqueous solutions of hen egg-white lysozyme display increased viscosity with concentration and reduced viscosity at higher temperatures (5°C to 55°C) [12]. High-concentration monoclonal antibody (MAb) solutions, commonly used in pharmaceutical formulations, exhibit exponential viscosity changes with protein concentration and temperature, with much higher viscosities at lower temperatures (2–8°C) compared to ambient temperature (25°C) [11] . Polymer solutions, such as xanthan gum and hydroxyethyl cellulose, also demonstrate shear-thinning behavior that becomes more pronounced at higher concentrations and lower temperatures [13]. Likewise, hydrogel formulations like Carbopol gels, used in topical applications, display increased viscosity at higher polymer concentrations, while temperature reduces viscosity and modifies their shear-thinning properties [14]. Even biological systems like blood exhibit non-Newtonian behavior, where viscosity increases with higher hematocrit and decreases with temperature. In all these cases, the interplay between concentration and temperature governs the complex, non-Newtonian viscosity profile of the system [15]. Building on the insights from previous investigations, we investigate the steady boundary layer flow of a Walter's B fluid driven by a stretching cylinder, where the viscosity varies with both temperature and concentration. The complex nonlinear problem is simplified into a system of ordinary differential equations through similarity transformations. The Reynolds model is applied throughout the study to describe the temperature and concentration-dependent variable viscosity. The physical effects of different parameters are illustrated in Tables 1, 2, and 3.

The structure of the paper is outlined as follows: Section 2 presents the formulation of the fluid flow model, including simplifications achieved through similarity transformations. Section 3 focuses on numerical simulations to analyze the model under varying parameter conditions, accompanied by graphical interpretations. Finally, Section 4 concludes the study by summarizing key findings and providing a comparative analysis with existing research.

2. Model Formulation

Consider the steady flow of an incompressible Walter's B fluid driven in the axial direction along a tube of radius a, with the $z-$axis aligned along the length of the tube and r representing the radial coordinate. The flow is induced by the stretching of the tube, leading to motion predominantly in the $z-$direction. Under these assumptions, the velocity field is axisymmetric, and the effects of the viscoelastic nature of Walter's B fluid are incorporated into the governing equations. The temperature of the surrounding fluid is T_1, where $T_w > T_1$, and the tube's surface is kept at T_w. Below are the governing equations:

$$\frac{\partial(rw)}{\partial z}+\frac{\partial(ru)}{\partial r}=0, \tag{2.1}$$

$$\begin{aligned}\rho\left(u\frac{\partial u}{\partial r}+w\frac{\partial u}{\partial z}\right)=&\frac{2\eta_0}{r}\frac{\partial u}{\partial r}-\frac{2k_0}{r}u\frac{\partial^2 u}{\partial r^2}-\frac{2k_0}{r}w\frac{\partial^2 u}{\partial z\partial r}+\frac{\partial}{\partial r}\left(2\eta_0\frac{\partial u}{\partial r}-2k_0u\frac{\partial^2 u}{\partial r^2}-2k_0w\frac{\partial^2 u}{\partial z\partial r}\right)\\&-\frac{\partial}{\partial z}\left(\eta_0\left(\frac{\partial u}{\partial z}+\frac{\partial w}{\partial r}\right)-k_0u\left(\frac{\partial^2 u}{\partial r\partial z}+\frac{\partial^2 w}{\partial r^2}\right)-k_0w\left(\frac{\partial^2 u}{\partial z^2}+\frac{\partial^2 w}{\partial z\partial r}\right)\right)\\&-2\eta_0\frac{u}{r^2}-2k_0\frac{u^2}{r^3}-\frac{2k_0}{r^2}\frac{\partial u}{\partial z},\end{aligned} \tag{2.2}$$

$$\begin{aligned}\rho\left(u\frac{\partial w}{\partial r}+w\frac{\partial w}{\partial z}\right)=&\frac{1}{r}\left(\eta_0\left(\frac{\partial u}{\partial z}+\frac{\partial w}{\partial r}\right)-k_0u\left(\frac{\partial^2 u}{\partial r\partial z}+\frac{\partial^2 w}{\partial r^2}\right)-k_0w\left(\frac{\partial^2 u}{\partial z^2}+\frac{\partial^2 w}{\partial z\partial r}\right)\right)+\\&\frac{\partial}{\partial r}\left(\eta_0\left(\frac{\partial u}{\partial z}+\frac{\partial w}{\partial r}\right)-k_0u\left(\frac{\partial^2 u}{\partial r\partial z}+\frac{\partial^2 w}{\partial r^2}\right)-k_0w\left(\frac{\partial^2 u}{\partial z^2}+\frac{\partial^2 w}{\partial z\partial r}\right)\right)+\\&\frac{\partial}{\partial z}\left(\eta_0\left(\frac{\partial u}{\partial z}+\frac{\partial w}{\partial r}\right)-2k_0u\frac{\partial^2 w}{\partial r\partial z}-2k_0w\frac{\partial^2 w}{\partial^2 z}\right),\end{aligned} \tag{2.3}$$

$$u\frac{\partial T}{\partial r}+w\frac{\partial T}{\partial z}=\alpha\left(\frac{\partial^2 T}{\partial r^2}+\frac{1}{r}\frac{\partial T}{\partial r}\right)+Q_0-\frac{\partial q_r}{\partial r}, \tag{2.4}$$

$$u\frac{\partial C}{\partial r}+w\frac{\partial C}{\partial z}=D\left(\frac{\partial^2 C}{\partial r^2}+\frac{1}{r}\frac{\partial C}{\partial r}\right), \tag{2.5}$$

Above system is governed by the following boundary conditions:

$$\begin{gathered}u=0, w=w_w, T=T_w\ , C=C_w \text{ at } r=a.\\ u\to 0,\ w\to 0,\ T\to T_\infty,\ C\to C_\infty \text{ as } r\to\infty.\end{gathered}$$

Here, u and w denote the velocity components in the radial (r) and axial (z) directions, respectively. The axial velocity at the wall is given by $w_w = 2cz$, where c is a positive constant representing the stretching rate of the tube. The parameters α, ν, ρ, T, k, and μ correspond to the thermal diffusivity, kinematic viscosity, fluid density, temperature, thermal conductivity, and dynamic viscosity of the fluid, respectively. The parameter Q_0 represents the heat generation within the system, while D denotes the diffusion coefficient used in the species transport equation, indicating the rate at which a chemical species spreads through the fluid. In this analysis, the radiative heat flux in the x-direction is considered negligible in comparison to the flux in the y-direction. Applying the Rosseland approximation for thermal radiation, the radiative heat flux q_r is expressed as:

$$q_r=-\frac{16\sigma T_0^3}{3k}\frac{\partial T}{\partial y},$$

where σ is the Stefan–Boltzmann constant, and k stands for the mean absorption coefficient. Under the following similarity transformations

$$\eta=\left(\frac{r}{a}\right)^2,\quad u=\frac{-ca}{\sqrt{\eta}}f(\eta),\quad w=2czf'(\eta),\quad \theta(\eta)=\frac{T-T_\infty}{T_w-T_\infty},\quad \phi(\eta)=\frac{C-C_\infty}{C_w-C_\infty}.$$

The dimensionless formulation that characterizes the boundary flow is expressed as

$$\begin{aligned}\eta_0(Re)\eta^2(ff''-f'^2)+2\eta_0\eta(f''+f''')+2A\eta f''f'''+2A(f'')^2+4Anff'''+4A\eta^2ff''''\\-A\eta ff''-2A\eta f'f''=0\end{aligned} \tag{2.6}$$

$$\theta'(\eta)\left(1+\frac{1}{2}RePrf(\eta)+\frac{8\sigma T_0^3}{3\alpha k}\right)+\left(\eta+\frac{16\eta\sigma T_0^3}{3\alpha k}\right)\theta''(\eta)=-\frac{a^2Q_0}{4\alpha\left(T_{\mathrm{w}}-T_\infty\right)} \tag{2.7}$$

$$\eta\phi'' + (1 + \frac{1}{2}ReScf(\eta))\phi' = 0 \tag{2.8}$$

Here, the prime indicates differentiation with respect to η, and the dimensionless parameters are defined as follows:

$$Re = \frac{ca^2}{\nu}, Pr = \frac{\nu}{\alpha}, A = \frac{k_0 c}{\eta_0}.$$

subject to the boundary conditions

$$f(1) = 0, f'(1) = 1, \theta(1) = 1, \phi(1) = 1, f(\infty) = 0, f'(\infty) = 0, \theta(\infty) = 0, \phi(\infty) = 0.$$

Here, the temperature-dependent viscosity is modeled as

$$\eta_0 = e^{-(P\theta + Q\phi)},$$

which, using the Maclaurin series expansion, can be approximated as

$$\eta_0 \approx 1 - P\theta - Q\phi + \mathcal{O}(\theta^2, \phi^2).$$

It is important to note that the case $M = 0$ corresponds to constant viscosity. Substituting the above expression into equations (2.6)-(2.8) yields the modified governing system.

$$\begin{aligned}(1 - P\theta - Q\phi)(Re)\eta^2(ff'' - f'^2) + 2(1 - P\theta)\eta(f'' + f''') + 2A\eta f''f''' + 2A(f'')^2 \\ + 4Anff''' + 4A\eta^2 ff'''' - A\eta ff'' - 2A\eta f'f'' = 0\end{aligned} \tag{2.9}$$

$$\theta'(\eta)\left(1 + \frac{1}{2}RePrf(\eta) + \frac{8\sigma T_0^3}{3\alpha k}\right) + \left(\eta + \frac{16\eta\sigma T_0^3}{3\alpha k}\right)\theta''(\eta) = -\frac{a^2 Q_0}{4\alpha\,(T_w - T_\infty)} \tag{2.10}$$

$$\eta\phi'' + (1 + \frac{1}{2}ReScf(\eta))\phi' = 0 \tag{2.11}$$

subject to the boundary conditions

$$f(1) = 0, f'(1) = 1, \theta(1) = 1, \phi(1) = 1, f(\infty) = 0, f'(\infty) = 0, \theta(\infty) = 0, \phi(\infty) = 0.$$

3. Results and discussions

In this section, numerical simulations are carried out to investigate the influence of various flow parameters on the velocity, temperature, and concentration profiles using MATLAB's built-in boundary value problem solver `bvp4c`. For the simulations, the following default parameter values are used: $A = 0.1$, $Re = 0.2$, $Pr = 1$, $Sc = 0.1$, $P = 0.1$, $Q = 0.1$, $k = 1$, $a = 1$, $\alpha = 0.1$, $\sigma = 0.5$, $T_w = 0.02$, $T_\infty = 0.5$, $Q_0 = 0.8$, $T_0 = 0.4$. The effects of key flow parameters on fluid behavior are analyzed, including the Prandtl number (Pr), Reynolds number (Re), Walter's B fluid parameter (A), Schmidt number (Sc), mean absorption coefficient (k), heat generation parameter (Q_0), and the Stefan–Boltzmann constant (σ). Figure 1 illustrates the variation in velocity with different values of A, showing that the velocity decreases as A increases. Figure 2 presents the $f(\eta)$ profile for varying values of A, highlighting the corresponding changes in the flow behavior. Similarly, Figure 3 displays the velocity variation for different values of Re, indicating that an increase in Re leads to a reduction in fluid velocity. This trend is further supported by Figure 4, which shows the $f(\eta)$ profile for various values of the Reynolds number. The flow of fluid is greatly influenced by the resistance it encounters while moving over a solid surface due to viscosity, resulting in a drag force known as skin friction that opposes the motion. This force plays a vital role in fluid dynamics, significantly affecting the behavior

and characteristics of fluid flow during its interaction with solid boundaries. In Table 1, the variation of skin friction for varying parameters A, Re, σ and k is presented. As A increases, skin friction rises accordingly. This indicates that the growing elasticity of the fluid with higher A amplifies the shear stress at the surface, leading to an increase in skin friction. Likewise, as the Reynolds number (Re) increases, skin friction also rises, indicating that the flow is likely transitioning to or has entered a turbulent regime, where increased boundary layer activity results in higher shear stress at the surface. In contrast, as the Stefan–Boltzmann constant (σ) increases, skin friction decreases. This suggests that enhanced radiative heat transfer reduces the viscosity near the surface, weakening the shear stress at the boundary. The increase in (σ) raises the temperature, lowering the fluid's viscosity and decreasing resistance to flow, ultimately reducing skin friction. This behavior highlights the dominant influence of thermal effects from increased radiation in modifying boundary layer dynamics and reducing surface drag. Additionally, the mean absorption coefficient (k) affects fluid velocity by controlling the rate of radiative heat transfer. As k increases, the fluid absorbs more thermal radiation, raising the temperature, which reduces viscosity and facilitates smoother fluid motion, potentially increasing the velocity.

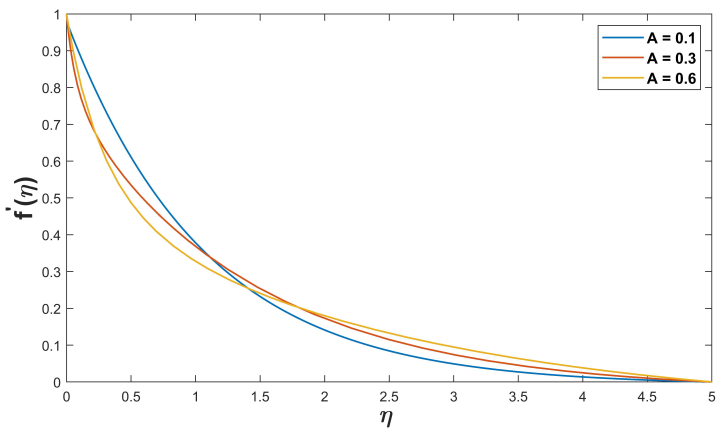

Figure 1: $f'(\eta)$ against different values of A.

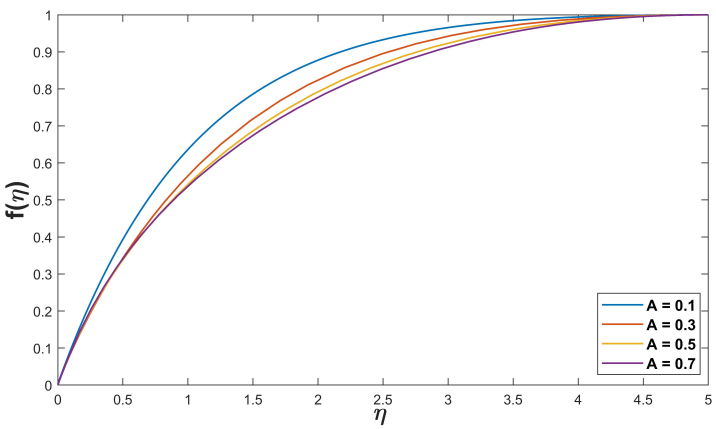

Figure 2: $f(\eta)$ against different values of A.

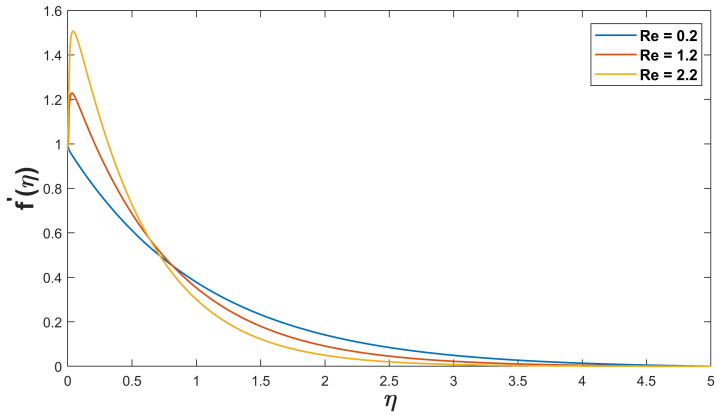

Figure 3: $f'(\eta)$ against different values of Re.

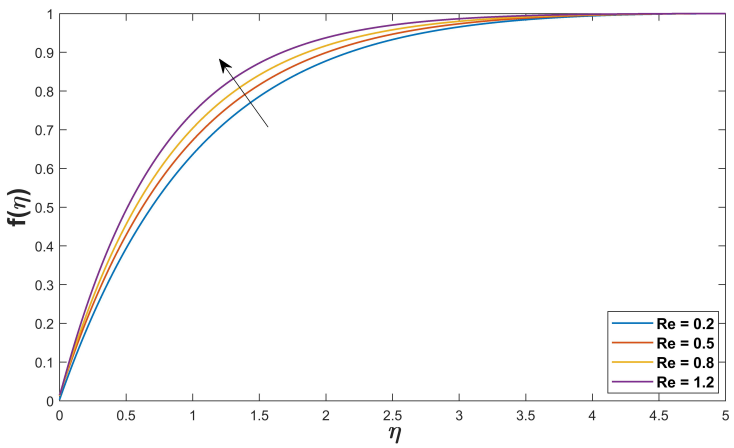

Figure 4: $f(\eta)$ against different values of Re.

A	c_f	Re	c_f	σ	c_f	k	c_f
0.1	-0.8440	0.1	-0.7429	0.5	-0.4505	1	-0.4505
0.3	-0.1882	0.2	-0.7389	0.7	-0.6613	2	-0.6611
0.5	-0.1211	0.3	-0.7366	0.9	-0.7389	3	-0.7390
0.7	-0.1036	–	–	1.2	-0.8250	4	-0.8244

Table 1: Skin friction (C_f) for variation of A, Re, σ and k.

Figures 5, 6, 7, and 8 provide a comprehensive analysis of how different parameters influence the temperature distribution within the flow field. Figure 5 illustrates the temperature profile for various values of the Prandtl number (Pr), showing that as Pr increases, the fluid temperature decreases. Figure 6 presents the temperature profile for varying values of A, indicating that temperature decreases with increasing A, likely due to enhanced energy dissipation that reduces temperature within the boundary layer. Likewise, Figure 7 illustrates the temperature profile for different values of the Reynolds number (Re), revealing that as Re increases, the fluid temperature decreases. This behavior is attributed to stronger convection at higher Re, which facilitates heat transfer away from the surface, lowering the fluid

temperature. A comparable pattern is observed with increasing values of the Stefan–Boltzmann constant (σ) and the mean absorption coefficient (k), where stronger radiative heat transfer leads to a decline in the fluid temperature, as depicted in Figures 9 and 10. Conversely, Figure 8 illustrates that a rise in the heat generation parameter (Q_0) results in an elevated temperature distribution within the fluid, due to the introduction of additional thermal energy. Table 2 presents the variation of the Nusselt number for different values of Pr, A, Re, and Q_0. An increase in the Prandtl number (Pr) leads to a higher Nusselt number, as lower thermal diffusivity intensifies the temperature gradient at the surface, thereby enhancing heat transfer. A similar enhancement is observed with increasing values of the Walter's B fluid parameter (A), where viscoelastic properties improve energy transport and support stronger convective heat transfer.

Moreover, an increase in the Reynolds number (Re) also contributes to an elevated Nusselt number, as intensified inertial effects promote enhanced convective transport near the boundary. In contrast, higher values of the heat generation parameter (Q_0) reduce the Nusselt number, since internal heat production diminishes the thermal gradient at the wall, thereby lowering the surface heat transfer rate.

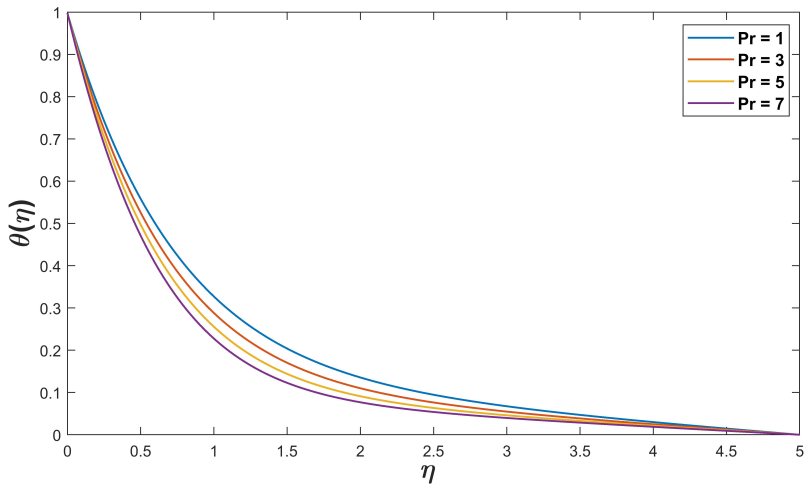

Figure 5: $\theta(\eta)$ against different values of Pr.

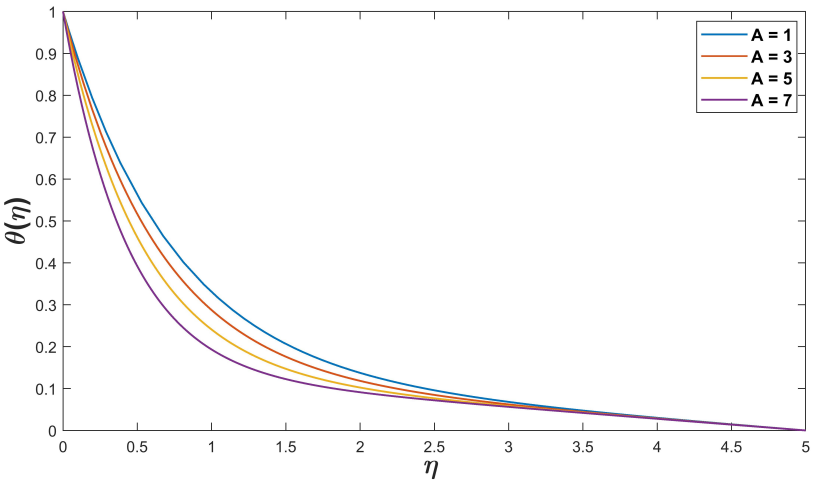

Figure 6: $\theta(\eta)$ against different values of A.

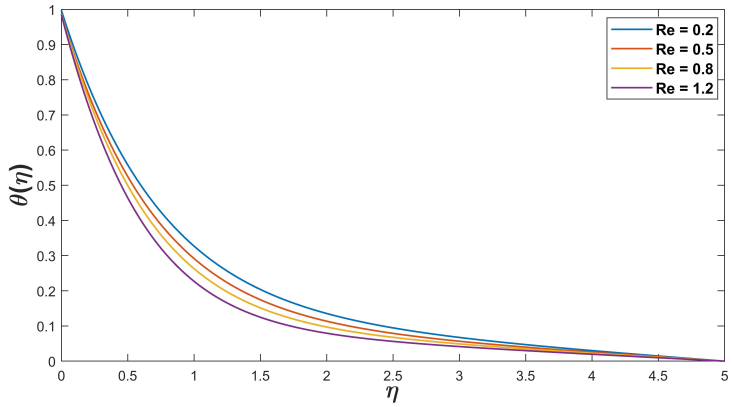

Figure 7: $\theta(\eta)$ against different values of Re.

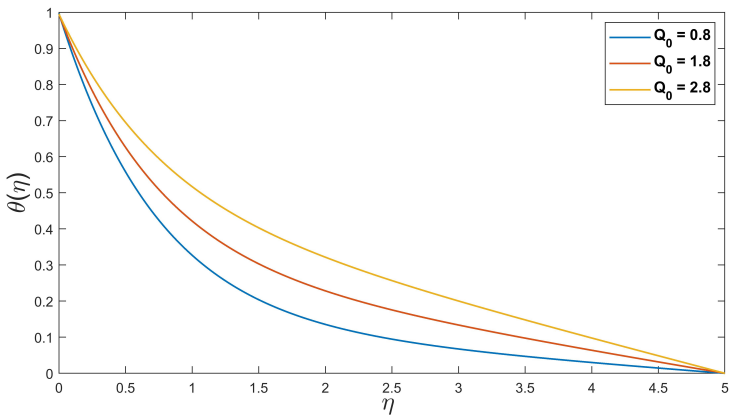

Figure 8: $\theta(\eta)$ against different values of Q_0.

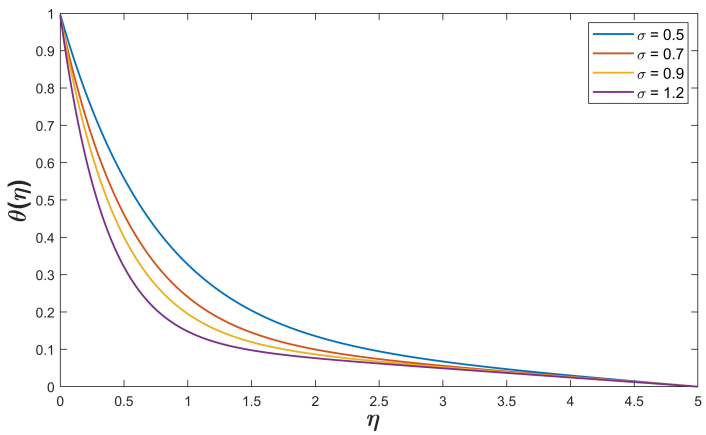

Figure 9: $\theta(\eta)$ against different values of σ.

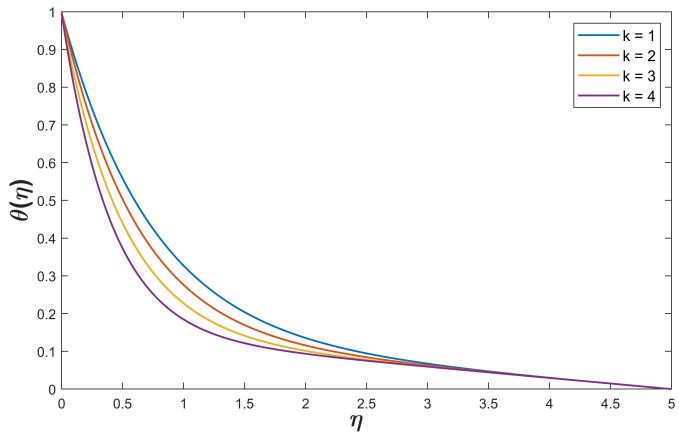

Figure 10: $\theta(\eta)$ against different values of k.

Pr	Nu	A	Nu	Re	Nu	Q_0	Nu
1	1.6291	1	1.1856	0.2	1.6291	0.8	1.6291
3	1.7471	3	1.3726	0.5	1.7320	1.8	1.3362
5	1.8542	5	1.6345	0.8	1.8194	2.8	1.0434
7	1.9527	7	2.0264	1.2	1.9368	–	–

Table 2: Nusselt Number (N_u) for variation of Pr, A, Re and Q_0

The variations in fluid concentration for different values of Re and Sc are illustrated in Figures 11 and 12. Figure 11 presents the concentration profile for varying Reynolds numbers (Re), demonstrating that fluid concentration decreases as Re increases. This occurs because higher Re enhances the convective transport, which accelerates the removal of solute particles from the flow, thereby reducing concentration. A similar trend is observed in Figure 12 for increasing values of the Schmidt number (Sc), where higher Sc results in lower concentration. This is because an increase in Sc corresponds to a decrease in mass diffusivity, which slows down molecular diffusion and limits the spread of the diffusing species, thereby reducing the concentration. This behavior suggests that heavier diffusing species exert a stronger retarding effect on the concentration distribution within the flow field. Table 3 presents the variation of the Sherwood number with respect to the parameters Re and Sc. As Re increases, the Sherwood number increases because stronger convection at higher Re enhances mass transfer near the boundary, promoting the removal of solute particles from the surface. As the Schmidt number Sc increases, the mass diffusivity of the species decreases, causing the concentration boundary layer to become thinner. This results in a steeper concentration gradient at the surface, which enhances the convective mass transfer rate and thereby increases the Sherwood number.

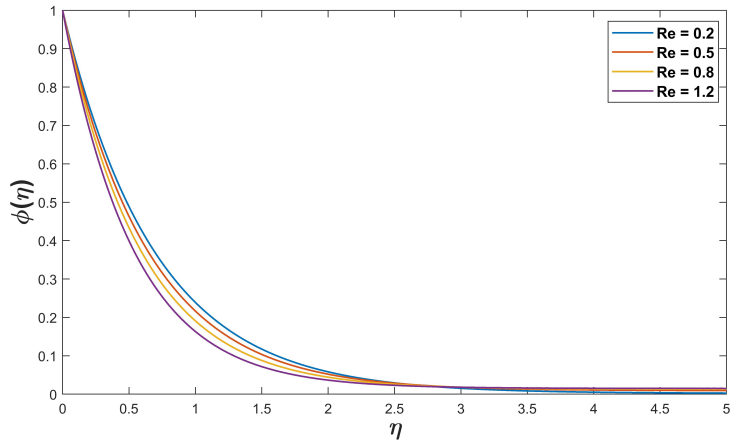

Figure 11: $\phi(\eta)$ against different values of Re.

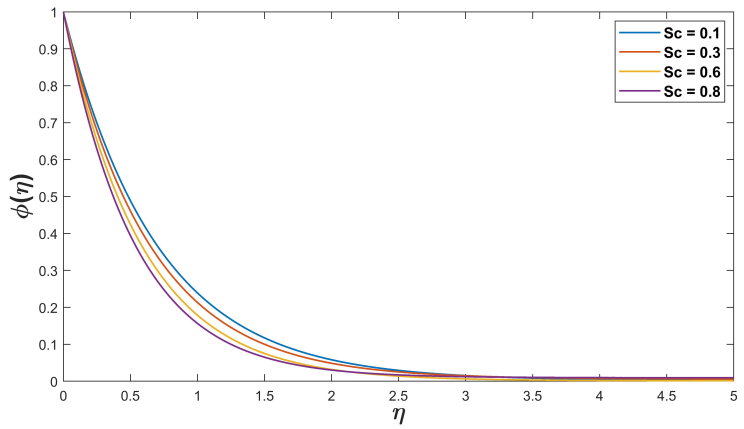

Figure 12: $\phi(\eta)$ against different values of Sc.

Re	Sh	Sc	Sh
0.2	1.9788	0.1	1.9788
0.5	2.0071	0.3	1.9925
0.8	2.0075	0.6	2.0126
1.2	2.0157	0.8	2.0259

Table 3: Sherwood Number (S_h) for variation of Re and S_c.

4. Conclusion

In this study, we explored the steady boundary layer flow of a Walter's B fluid induced by a stretching cylinder, where the viscosity depends on both temperature and concentration. By applying standard similarity transformations, the governing equations were reduced to a system of nonlinear ordinary differential equations. To obtain more precise and detailed solutions, we utilized MATLAB's 'BVP4c' solver. Our numerical investigations aimed to provide valuable insights into the system's behavior, offering critical information for optimizing processes and designs across various fields, including engineering, environmental science, and materials science. The numerical analysis yielded the following key findings:

1. Fluid velocity decreases with increasing values of the parameter A, indicating that higher elasticity of the fluid increases resistance to flow.
2. As the Reynolds number (Re) increases, fluid velocity decreases due to enhanced inertial effects that dominate over viscous forces.
3. Fluid temperature decreases with higher Prandtl numbers (Pr), as stronger thermal diffusion reduces heat retention.
4. Increasing the parameter A leads to a decrease in fluid temperature, likely due to enhanced energy dissipation in the fluid.
5. Higher Reynolds numbers (Re) result in lower fluid temperatures, attributed to increased convective heat transfer.
6. An increase in the Stefan–Boltzmann constant (σ) and the mean absorption coefficient (k) reduces the fluid temperature by enhancing radiative heat transfer.
7. A rise in the heat generation parameter (Q_0) increases the fluid temperature due to additional heat introduced into the system.
8. Fluid concentration decreases with increasing Reynolds number (Re), as stronger convection enhances the removal of solute particles.
9. Higher Schmidt numbers (Sc) lead to lower concentration, as reduced mass diffusivity slows down the spread of diffusing species.

To verify the accuracy of our analysis, we compared our results with those reported by Hussain et al. [16], who carried out an analytical study on the steady boundary layer flow of a Walter's B fluid driven by a stretching cylinder. Their work considered temperature-dependent variable viscosity and employed the homotopy analysis method (HAM), with a primary focus on velocity and heat transfer characteristics. In contrast, our model extends the analysis by addressing both heat and mass transfer, incorporating viscosity variations that depend on both temperature and concentration.

Our results show consistency with the trends reported in [16] for key quantities such as skin friction, the Nusselt number, and the Sherwood number across a range of parameter values. The inclusion of concentration-dependent viscosity and thermal radiation effects using the Rosseland approximation distinguishes our model and enhances its relevance. We anticipate that this extended framework will attract considerable interest from researchers working in non-Newtonian fluid dynamics and heat/mass transfer phenomena.

Nomenclature

u and w	the velocity components in the r and z directions (m/s).
r	axis along radial direction (m).
ρ	fluid density $(kg.m^{-}3)$
η_0	zero-shear viscosity (or dynamic viscosity) $(Pa.s = kg/(m.s))$
T	fluid temperature (K (Kelvin))
k_0	elastic parameter (or Walter's B fluid parameter) (m^2/s)
α	thermal diffusivity (m^2/s)
Q_0	heat generation parameter $(J/(m^3.s))$.
q_r	radiative heat flux $(J/(m^2.s))$
μ	viscosity of the fluid $(Pa.s = kg/(m.s))$
ν	kinematic viscosity (m^2/s).
C	concentration of the species (Kg/m^3)
D	diffusion coefficient (m^2/s)
σ	Stefan–Boltzmann constant $(W/m^2.K^4)$.
k	mean absorption coefficient $(m^{-}1)$.

Acknowledgments

We extend our sincere appreciation to the referees for their thoughtful suggestions that contributed to the improvement of this paper.

Conflict of Interest

The authors affirm that there are no financial or personal connections that could have improperly influenced the content or conclusions presented in this manuscript.

References

1. Mehrotra, A. K., Svrcek, W. Y., *Viscosity of compressed Athabasca bitumen*, Can. J. Chem. Eng., 64(5), 844-847, (1986).
2. Chhabra, R. P., Richardson, J. F., *Non-Newtonian flow and applied rheology: engineering applications*, Butterworth-Heinemann, (2011).
3. Massoudi, M., Christie, I., *Effect of variable viscosity and viscous dissipation on the flow of a third grade fluid in a pipe*, Int. J. Non-Lin. Mech., 30, 687–699,(1995).
4. Hayat, T., Ellahi, R., Asghar, S., *The influence of variable viscosity and viscous dissipation on the non-Newtonian flow: an analytic solution*, Commun. Nonlin. Sci. Numer. Simulat., 12, 300–313, (2007).
5. Yurusoy, M., Pakdermirli, M., *Approximate analytical solutions for flow of a third grade fluid in a pipe*, Int. J. Non-Lin. Mech., 37, 187–195, (2002).
6. Pakdermirli, M., Yilbas, B.S., *Entropy generation for pipe flow of a third grade fluid with Vogel model of viscosity*, Int. J. Non-Lin. Mech., 41, 432–437, (2006).
7. Nadeem S., Ali M., *Analytical solutions for pipe flow of a fourth grade fluid with Reynold and Vogel's models of viscosities*, Commun. Nonlin. Sci. Numer. Simulat., 14, 2070–2090, (2009).
8. Nadeem, S., Hayat, T., Abbasbandy, S., Ali, M., *Effects of partial slip on a fourth-grade fluid with variable viscosity: an analytical solution*, Nonlin. Anal.: Real World Appl. 11 856–868, (2010).
9. Nadeem, S., Akbar, N.S., *Effects of temperature-dependent viscosity on peristaltic flow of a Jeffrey-six constant fluid in a non-uniform vertical tube*, Commun. Nonlin. Sci. Numer. Simulat., 15, 3950, (2010).
10. King, D. M., Wang, Z., Kendig, J. W., Palmer, H. J., Holm, B. A., Notter, R. H., *Concentration-dependent, temperature-dependent non-Newtonian viscosity of lung surfactant dispersions*, Chem. Phys. Lipids, 112(1), 11-19, (2001).
11. Palm, T., Sahin, E., Gandhi, R., Khossravi, M., *The importance of the concentration-temperature-viscosity relationship for the development of biologics*, Bio. Process. Int., 10, (2015).
12. Monkos, K., *Concentration and temperature dependence of viscosity in lysozyme aqueous solutions*. Biochim. Biophys. Acta, 1339(2), 304-310, (1997).
13. Lapasin, R. *Rheology of industrial polysaccharides: theory and applications*, Springer Science & Business Media, (2012).
14. Barry, B. W., Meyer, M. C., *The rheological properties of carbopol gels I. Continuous shear and creep properties of carbopol gels*, Int. J. Pharm., 2(1), 1-25, (1979).
15. Baskurt, O. K., Meiselman, H. J., *Blood rheology and hemodynamics*, In Seminars in Thrombosis and Hemostasis, 29(05), 435-450, (2003). Copyright© 2003 by Thieme Medical Publishers, Inc., 333 Seventh Avenue, New York, NY 10001, USA.
16. Hussain, A., Ullah, A., *Boundary layer flow of a Walter's B fluid due to a stretching cylinder with temperature dependent viscosity*, Alex. Eng. J., 55(4), 3073-3080, (2016).

Annwesha Borthakur,
Department of Mathematics,
Dibrugarh University,
India.
E-mail address: annbor040@gmail.com

and

Debasish Dey,
Department of Mathematics,
Dibrugarh University,
India.
E-mail address: debasishdey1@dibru.ac.in